

# Instability and Spatiotemporal Dynamics of Alternans in Paced Cardiac Tissue

Blas Echebarria and Alain Karma

*Department of Physics and Center for Interdisciplinary Research on Complex Systems,  
Northeastern University, Boston, MA 02115*

(November 23, 2001)

We derive an equation that governs the spatiotemporal dynamics of small amplitude alternans in paced cardiac tissue. We show that a pattern-forming linear instability leads to the spontaneous formation of stationary or traveling waves whose nodes divide the tissue into regions with opposite phase of oscillation of action potential duration. This instability is important because it creates dynamically an heterogeneous electrical substrate for inducing fibrillation if the tissue size exceeds a fraction of the pattern wavelength. We compute this wavelength analytically as a function of three basic length scales characterizing dispersion and inter-cellular electrical coupling.

PACS numbers: 87.19.Hh, 05.45.-a, 05.45.Gg, 89.75.-k

It is well established that the duration of cardiac excitation can oscillate from beat to beat at sufficiently short pacing interval [1]. Pioneering studies by Nolasco and Dahlen [2] and Guevara *et al.* [3] have demonstrated that the generic sequence LSLS... of long and short action potential duration (*APD*), known as alternans, is a direct consequence of the restitution relationship

$$APD^{n+1} = f(DI^n) \quad (1)$$

between the *APD* generated by the  $n^{th} + 1$  stimulus,  $APD^{n+1}$ , and the diastolic time interval  $DI^n$  during which the tissue recovers its resting properties after the end of the previous ( $n^{th}$ ) action potential. If we denote the interval between the  $n^{th}$  and  $n^{th} + 1$  stimulus by  $T^n$ , we must have  $DI^n = T^n - APD^n$ . Then, for a fixed period:  $T^n = \tau$  for all  $n$ , Eq. 1 yields the map  $APD^n = f(\tau - APD^{n-1})$  that has a period doubling instability if the slope  $f'$  of the restitution curve evaluated at its fixed point exceeds unity, which generically occurs as the period is decreased.

Over the last decade, the study of alternans [4–11], and their control [12], has become a main focus of research because of the potentially crucial link of this dynamical instability with cardiac fibrillation [13]. However, there is presently no simple analytical understanding of how the bifurcation to alternans is manifested *spatiotemporally* in paced cardiac tissue. Analytical progress to date is limited to the one-dimensional circulation of electrical impulse in a ring of tissue [5–7].

In this letter, we derive an equation that governs the spatiotemporal dynamics of alternans close to the onset of instability. This enables us to obtain a quantitative analytical understanding of the formation of recently observed complex patterns of *APD* oscillations that can promote fibrillation [8–11]. A crucial feature of these patterns is that the *APD* oscillates with opposite phases in two (or more) spatially extended regions of tissue, i.e. with a sequence LSLS... in one region and SLSL... in the other. These “discordant alternans” have been observed experimentally in both two-dimensional [8] and linear strands [9] of cardiac tissue, as well as in ionic model simulations [9–11]. Moreover, they have been shown to

lead to the formation of conduction blocks [9] as well as to the onset of spiral wave formation and fibrillation [8]. We show here that discordant alternans result from a *pattern-forming* linear instability that has interesting similarities with classic instabilities leading to the spontaneous formation of spatially periodic patterns in nature (such as Rayleigh-Bénard convection, Taylor-Couette flow, etc [14]), but also presents some unique features.

We consider a one-dimensional (1-d) homogeneous cable of length  $L$  paced at period  $\tau$  from one end ( $x = 0$ ). Close to the onset of instability, we can expand the *APD* and the period in the form

$$APD^n(x) \approx APD_c + a(x, t) e^{i\pi n}, \quad (2)$$

$$T^n(x) \approx \tau_c - \delta\tau + b(x, t) e^{i\pi n}, \quad (3)$$

where  $APD_c$  and  $\tau_c$  are the *APD* and the period evaluated at the bifurcation point of the map ( $f' = 1$ ),  $x$  measures the position along the cable, and  $\delta\tau \equiv \tau_c - \tau \ll \tau_c$ . In this range of period,  $a$  and  $b$  vary slowly from beat to beat, which allows us to treat the time,  $t \equiv n\tau$ , as a continuous variable; the fast beat-to-beat oscillations are contained in the exponential factor  $e^{i\pi n}$ .

A relation between  $a$  and  $b$  can first be derived by noting that  $T^n(x)$  is the difference of arrival time of two subsequent action potentials at  $x$  [11], or

$$T^n(x) = \tau + \int_0^x \frac{dx'}{c(DI^n(x'))} - \int_0^x \frac{dx'}{c(DI^{n-1}(x'))}, \quad (4)$$

where the first (second) integral on the right-hand-side is the time required for the leading front of the action potential to travel from the paced end to  $x$  at the  $n^{th}$  ( $n^{th} - 1$ ) stimulus; concomitantly,  $c(DI)$  is the standard dispersion curve that relates the propagation speed of this front with the local diastolic interval. The dispersion curve is typically steeply increasing at small  $DI$  and flat at large  $DI$ . Substituting Eqs. 2-3 in Eq. 4 with  $DI^n(x) = T^n(x) - APD^n(x)$ , and expanding to linear order in  $a$  and  $b$ , we obtain  $b(x) \simeq \int_0^x a(x') dx' / \Lambda$  where we have defined  $\Lambda \equiv c^2 / (2c')$ , with  $c$  and  $c' \equiv dc/dDI$  evaluated at the bifurcation, and assumed that  $\Lambda$  is much larger than the scale over which  $a$  varies.

Next, in order to derive an evolution equation for the amplitude  $a(x, t)$ , we first neglect the influence of the electrical coupling between cells on the *APD*. This allows us to assume that the restitution relationship (1), and hence the second iteration of the map

$$APD^{n+2} = f(T^{n+1} - f(T^n - APD^n)), \quad (5)$$

continues to be valid even when the *APD* is non-spatially uniform; we shall soon see why it is crucial to relax this assumption. We substitute Eqs. 2-3 in Eq. 5, and expand the right-hand-side keeping only the dominant linear and weakly nonlinear terms. Furthermore, we use the aforementioned fact that, close to onset,  $a$  varies slowly from beat to beat, and we therefore expand the left-hand-side as  $APD^{n+2} \simeq APD^n + 2 \partial a / \partial n e^{i\pi n}$ , where  $\partial a / \partial n = \tau \partial a / \partial t$ . Finally, we use the integral relation between  $a$  and  $b$  derived earlier. After equating both sides of Eq. 5, we obtain

$$\tau \partial_t a = \sigma a - g a^3 - \int_0^x \frac{dx'}{\Lambda} a(x'), \quad (6)$$

where  $\sigma \equiv f''(\tau - \tau_c)/2$ ,  $g \equiv f''^2/4 - f'''/6$ , and all derivatives are evaluated at the bifurcation point.

In order to test this evolution equation, we simulate the standard cable equation

$$\partial_t V = D \partial_x^2 V - (I_{ion} + I_{ext}) / C_m, \quad (7)$$

for the membrane current  $I_{ion}$  given by the Noble model [15] with time in units of millisecond (ms),  $D = 2.5 \times 10^{-4}$  cm<sup>2</sup>/ms,  $C_m = 12 \mu\text{F}/\text{cm}^2$ ,  $dx=0.01$  cm,  $dt=0.05$  ms, and  $I_{ext}$  modeling a sequence of stimuli applied at  $x = 0$  at the pacing interval  $\tau$ . To determine the parameters of the amplitude equation, we compute the restitution and dispersion curves by pacing Eq. 7 in a short cable and by using two subsequent stimuli spaced by different intervals to vary  $DI$ ; we also use  $V = -40$  mV as threshold of the transmembrane voltage to define the *APD*. We impose zero gradient boundary conditions on  $V$  and  $a$  at the two ends of the cable in all our simulations.

Fig. 1(a) shows that Eq. 6 produces discordant alternans consistent with the picture that restitution and dispersion suffice to produce this state [9–11]. However, the magnitude of the spatial gradient of  $a$  at the node increases with time, and can be shown to diverge in a finite time. This yields an unphysical spatial discontinuity of *APD*, which also occurs if the system of coupled maps (Eqs. 1 and 4), from which the amplitude equation is derived, is solved numerically. Note that the analogous system of coupled maps for a 1-d pulse circulating in a ring produces a smooth *APD* modulation starting from a smooth initial condition [5], which highlights the much stronger role of dispersion at producing heterogeneity of *APD* during pacing than circulation.

This discontinuity, which is absent in the simulation of the cable equation in Fig. 1(b), can be cured by adding spatial derivative terms to the amplitude equation. Since

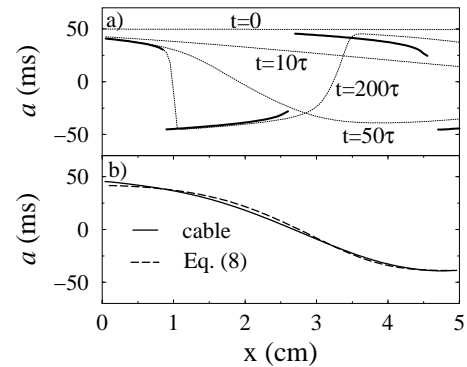


FIG. 1. Amplitude  $a$  of *APD* oscillation vs  $x$  for Noble parameters and  $\tau = 258$  ms. (a): profiles obtained with Eq. 6 at different times (dotted lines) and final stationary profile (solid line). (b): stationary profiles obtained with Eq. 7 (solid line) and Eq. 8 (dashed line). Nodes ( $a = 0$ ) separate tissue regions with  $\pi$  out of phase oscillations.

the cable is paced at one end, the underlying basic state (i.e. traveling pulses) is not invariant under parity symmetry. Hence, in addition to  $\partial_x^2 a$ , a term proportional to  $\partial_x a$  must generally be included, which yields the final form of our amplitude equation

$$\tau \partial_t a = \sigma a - g a^3 - \int_0^x \frac{dx'}{\Lambda} a(x') - w \partial_x a + \xi^2 \partial_x^2 a. \quad (8)$$

To calculate the new lengthscales  $w$  and  $\xi$ , we must determine how the electrical coupling between cells modifies the restitution relationship (Eq. 1). For complex electrophysiological models such as Noble, this generally needs to be done numerically using a procedure that will be discussed elsewhere. For a simple two-variable ionic model, which we study below, the analytical expressions

$$w = 2D/c, \quad (9)$$

$$\xi = (D \times APD_c)^{1/2}, \quad (10)$$

can be derived by interpreting Eq. 7 as a diffusion equation with a source  $I_{ion}$ , and expressing  $V$  as space-time integral of  $GI_{ion}$ , where  $G$  is the standard Green's function of the diffusion equation. This integral can then be evaluated analytically because the action potential shape is simply triangular for this model, and used to calculate  $w$  and  $\xi$ . Eq. 10 has the simple physical interpretation that  $V$  diffuses a length  $\sim \xi$  in the time interval of one *APD*. Therefore, the repolarization of a given cell is influenced by other cells within a length  $\sim \xi$  of cable. In addition, repolarization of this cell is influenced unequally by its left and right neighboring cells because these cells are activated at different times by the propagating wavefront. Clearly, this asymmetry must vanish in the limit  $c \rightarrow \infty$  where all cells are activated simultaneously consistent with Eq. 9. Fig. 1(b) shows that our regularized amplitude equation (8) now produces a smoothly varying stationary profile of  $a$  that agrees well

TABLE I. Values of various lengths in cm with  $\lambda_{theor}$  (Eq. 12 or Eq. 13) and  $\lambda_{sim}$  (from simulations of Eq. 7).

Model	$\Lambda$	$w$	$\xi$	$\lambda_{theor}/4$	$\lambda_{sim}/4$	$L_{min}$
Noble	49.1	0.045	0.18	2.33	2.6	2.75
Two-variable	3.55	0.031	0.235	1.33	1.1	1.15

with the simulation of the cable-Noble equation, where  $a$  is obtained from the *APD* using Eq. 2.

The genesis of discordant alternans can be understood by computing the linear stability spectrum of the spatially homogeneous state ( $a = 0$ ). We have calculated this spectrum both numerically for different  $L$ , and analytically for the large  $L$  limit. The main result is that the wave pattern can emerge from the amplification of *either* a unique finite wavelength mode, which yields a stationary pattern, *or* from a discrete set of complex modes that approach a continuum in the limit  $L \rightarrow \infty$ , and yields a traveling pattern. There is indeed experimental evidence for both stationary [8] and traveling [9] waves.

We treat here explicitly the large  $L$  limit since it provides the basis to understand finite- $L$  patterns. In this limit, we can analyze stability by differentiating Eq. 8 with respect to  $x$  and letting  $a(x, t) \sim e^{ikx + \Omega t}$ , with both  $\Omega \equiv \Omega_r + i\Omega_i$  and  $k \equiv k_r + ik_i$  complex, which yields at once the eigenvalue equation

$$\Omega = \sigma - \xi^2 k^2 - i[wk - 1/(\Lambda k)]. \quad (11)$$

When dispersion is weak, a unique real mode with  $k_i = 0$  grows faster than the other complex modes and yields a stationary pattern. Its wavelength  $\lambda = 2\pi/k_r$ , is determined by the condition  $\Omega_i = 0$ , which yields

$$\lambda = 2\pi(w\Lambda)^{1/2}, \quad (12)$$

in good agreement with the wavelength observed in simulations of the cable-Noble equation (Table I). Note that  $\cos k_r x$  is an exact eigenvector of Eq. 8 linearized around  $a = 0$  that satisfies  $\partial_x a = 0$  at the two cable ends when  $L$  is an integer multiple of  $\lambda/2$ . The threshold of instability occurs when  $\Omega_r = 0$ , or for a period  $\tau_{th}$  defined by  $\sigma_{th} = f''(\tau_{th} - \tau_c)/2 = \xi^2/(w\Lambda)$ .

In the opposite limit where dispersion is strong, complex modes that grow exponentially at large  $x$  are the most unstable. It is simple to deduce from Eq. 11 that each  $k$ -mode travels towards the pacing end of the cable, but a wave-packet constructed from a linear superposition of these modes has a group velocity that makes the packet move away from the pacing end. This is the signature of a convective instability [14] where perturbations are transported as they grow, similarly to Taylor-Couette vortices developing in an axial flow [16]. In such a situation, patterns are only transient unless the group velocity vanishes, or  $\partial\Omega_i/\partial k_r = 0$ , and hence they grow at a fixed point in space. Moreover, the fastest growing wavelength that dominates at large time must correspond to a maximum of  $\Omega_r$ , which yields the additional

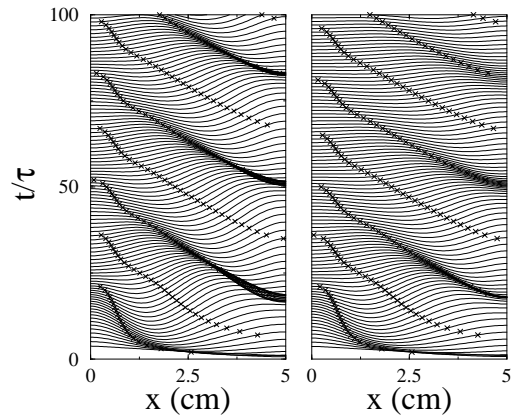


FIG. 2. Space-time plots of  $a$  obtained by simulations of Eq. 8 for parameters of the two-variable model, showing absolutely unstable (left and  $\tau = 295$  ms) and convectively unstable (right and  $\tau = 298$  ms) wave patterns. The crosses denote the positions of the nodes ( $a = 0$ ).

condition  $\partial\Omega_r/\partial k_r = 0$ . These two conditions are equivalent to requiring that  $d\Omega/dk = 0$ . From this, we deduce that the threshold of absolute instability occurs when  $\sigma_{th} = (3/2)(\xi/2\Lambda)^{2/3}$ , with a pattern of wavelength

$$\lambda = (4\pi/\sqrt{3})(2\xi^2\Lambda)^{1/3}, \quad (13)$$

which travels with phase velocity  $\Omega_i\lambda/(2\pi)$  where  $\Omega_i = (3\sqrt{3}/2)(\xi/2\Lambda)^{2/3}$ . It can also be deduced that traveling waves are favored over a stationary pattern when  $\Lambda = 2c^2/c' \ll \xi^4/w^3$ , and hence for large enough dispersion ( $c'$ ), and vice versa in the opposite limit.

Nonlinearities are mainly responsible for saturating the amplitude of the linear modes, but both the wavelength and evolution of the pattern can generally vary with distance from onset. There is a close analogy between the amplitude equation (8) and the real Ginzburg-Landau equation that has been extensively studied in the context of phase transitions and front propagation [14]. The dynamics is richer here because the integral term originating from dispersion causes a non-local interaction of the fronts separating two out-of-phase oscillating regions with the pacing end of the cable.

As a final test of our theory, we study a two-variable model where all the parameters of the amplitude equation can be calculated analytically including  $w$  and  $\xi$  given by Eqs. 9-10, and for which our theory predicts traveling waves. In this model,  $I_{ion}/C_m$  is the sum of a slow outward current,  $I_o/C_m = \tau_0^{-1}(S + (1-S)V/V_c)$ , and a fast inward current,  $I_i/C_m = -\tau_a^{-1}hS$ , where inactivation of the latter is controlled by

$$\partial_t h = (1 - S - h)/(\tau^-(1 - S) + S\tau^+) \quad (14)$$

In addition,  $V$  is dimensionless and  $S \equiv (1 + \tanh((V - V_c)/\epsilon))/2$ . We choose  $V_c = 0.1$ ,  $\tau_0 = 150$  ms,  $\tau_a = 6$  ms,  $\tau^- = 60$  ms,  $\tau^+ = 12$  ms,  $\epsilon = 0.005$ , and we simulate Eq. 7 with the same  $D$  as before,  $dx = 0.01$  cm,  $dt = 0.02$  ms, and  $V = 0.1$  as threshold for the *APD*.

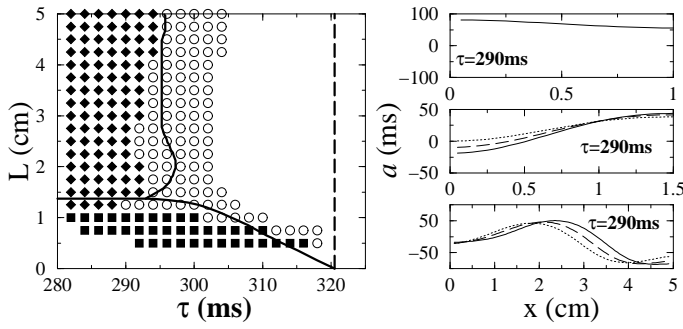


FIG. 3. Stability diagram of two-variable cable model with domains of no-alternans (open circles), concordant alternans (filled squares), and discordant alternans (filled diamonds); conduction blocks form at smaller  $\tau$  not shown here. Boundaries between the same domains obtained by simulations of the amplitude equation (8) are shown by solid lines. The dashed line denotes the bifurcation period for alternans predicted by the map of Eq. 1. On the right panel we show profiles of  $a$  vs  $x$  at times  $t$  (solid),  $t + 2\tau$  (dashed) and  $t + 4\tau$  (dotted lines), for three different cable lengths.

As predicted, we observe traveling waves in this model with a wavelength that agrees well with Eq. 13. Fig. 2 illustrates sustained and transient wave patterns above (left) and below (right) the onset of absolute stability, respectively. Furthermore, Fig. 3 shows that the results of simulations of the cable and amplitude equations are in good agreement over a wide range of  $L$  and  $\tau$ , including the fact that the onset of instability occurs at a shorter period in a larger cable (and, hence, for a slope of the restitution curve larger than unity). Fig. 3 is qualitatively similar for stationary waves, but this over-stabilization is smaller because dispersion is weaker.

The *APD* oscillations at a fixed  $x$  are periodic when the wave is stationary and quasiperiodic when it travels. For both cases, we find here that  $\lambda$  is independent of  $L$ , in contrast to the oscillations produced by a pulse circulating in a ring where it is known that  $\lambda \simeq 2L/(2i + 1)$  for weak dispersion [5] (with  $i$  integer and  $L$  = ring perimeter). As will be discussed elsewhere, our theory applied to the ring shows that the bifurcation to alternans is finite dimensional with  $i = 0$  being the most unstable mode, in agreement with the fact that it is this mode that is generically selected in experiments [4] and ionic model simulations [5–7]. In addition, it shows that the gradient term ( $-w\partial_x a$ ) can lead to quasiperiodicity even in the absence of dispersion ( $c' = 0$ ).

Our results demonstrate that the formation of discordant alternans is crucially affected by the effect of electrical coupling (diffusion) on repolarization, in addition to restitution and dispersion. Dispersion is responsible for the formation of nodes and spatial gradients of *APD* that steepen with time. Diffusion, in turn, tends to spread the *APD* spatially, and also induces a drift of the pattern away from the pacing site that is induced by the more subtle gradient term ( $-w\partial_x a$ ) in the amplitude equation.

When dispersion is sufficiently weak, drift balances dispersion and produce a stationary pattern. In the opposite limit, the tendency for dispersion to form steep gradients of *APD* is balanced by the spreading effect of diffusion. Nodes then travel, cyclically disappearing (appearing) at the pacing (opposite) end of the cable.

In conclusion, we have derived a simple evolution equation that describes the universal spatiotemporal dynamics of small amplitude alternans in paced cardiac tissue. Moreover, we have shown that discordant wave patterns [8–11], which are linked to fibrillation [8], result from a finite wavelength linear instability. Hence, their formation requires a minimum tissue size  $L_{min} \sim \lambda/4$ , required for at least one node to form. The value of  $L_{min}$  that we measure in simulations of reaction-diffusion models are actually close to  $\lambda/4$  with  $\lambda$  predicted by Eq. 12 and Eq. 13, respectively (Table I). This equation can be extended to higher dimensions as well as to include heterogeneities. Our preliminary results in a 2-d homogeneous tissue are very similar to 1-d. Finally, this equation is readily applicable to model a non-constant pacing interval and provides a theoretical basis to study the control of alternans in spatially extended tissue.

This research was supported in part by NIH SCOR in Sudden Cardiac Death P50-HL52319.

- 
- [1] G. R. Mines, *J. Physiol. (Lond.)* **46**, 349 (1913).
  - [2] J. B. Nolasco and R. W. Dahlen, *J. App. Physiol.* **25**, 191 (1968).
  - [3] M. R. Guevara *et al.*, in *Computers in Cardiology*, IEEE Comp. Soc., pp. 167 (1984).
  - [4] L. H. Frame and M. B. Simson, *Circulation* **78**, 1277 (1988).
  - [5] M. Courtemanche, L. Glass and J. P. Keener, *Phys. Rev. Lett.* **70**, 2182 (1993).
  - [6] A. Karma, *Chaos* **4**, 461 (1994).
  - [7] A. Vinet, *Annals Biomed. Eng.* **28**, 704 (2000).
  - [8] J. M. Pastore *et al.*, *Circulation* **99**, 1385 (1999).
  - [9] J. J. Fox *et al.*, *Spatiotemporal Transition to Conduction Block in Canine Ventricle*, *Circ. Res.*, in press.
  - [10] Z. Qu *et al.*, *Circ. Res.* **102**, 1664 (2000).
  - [11] M. A. Watanabe *et al.*, *J. Cardiovasc. Electrophys.* **12**, 196 (2001).
  - [12] K. Hall *et al.* *Phys. Rev. Lett.* **78**, 4518 (1997); D. J. Gauthier and J. E. S. Scooliar, *Phys. Rev. Lett.* **79**, 4938 (1997); D. J. Christini *et al.*, *Proc. Nat. Acad. Sci.* **98**, 5827 (2001).
  - [13] See: A. Karma, *Proc. Natl. Acad. Sci USA* **97**, 5687 (2000); D. S. Rosenbaum, *J. Cardiovasc. Electrophysiol.* **12**, 207 (2001); and earlier references therein.
  - [14] M. C. Cross and P. C. Hohenberg, *Rev. Mod. Phys.* **65**, 851 (1993).
  - [15] D. Noble, *J. Physiol* **160**, 317 (1962).
  - [16] K. L. Babcock, G. Ahlers, and D. S. Cannell, *Phys. Rev. Lett.* **67**, 3388 (1991).